

A tunable phonon–exciton Fano system in bilayer graphene

Tsung-Ta Tang^{1†}, Yuanbo Zhang^{1†‡}, Cheol-Hwan Park¹, Baisong Geng^{1,2}, Caglar Girit¹, Zhao Hao^{3,5}, Michael C. Martin³, Alex Zettl^{1,4}, Michael F. Crommie^{1,4}, Steven G. Louie^{1,4}, Y. Ron Shen^{1,4} and Feng Wang^{1,4*}

Fano resonances are features in absorption, scattering or transport spectra resulting from the interaction of discrete and continuum states. They have been observed in a variety of systems^{1–6}. Here, we report a many-body Fano resonance in bilayer graphene that is continuously tunable by means of electrical gating. Discrete phonons and continuous exciton (electron–hole pair) transitions are coupled by electron–phonon interactions, yielding a new hybrid phonon–exciton excited state. It may also be possible to control the phonon–exciton coupling with an optical field. This tunable phonon–exciton system could allow novel applications such as phonon lasers.

Two-dimensional graphene shows remarkable electrical^{7,8}, vibrational^{9–12} and optical properties^{13–17}. Many of these properties can be modified in graphene by means of electrical gating, which allows control of the intricate interplay between electrons, phonons and photons. Such control is exemplified in gated bilayer graphene structures in which a gating electrical field can modify phonon–light interactions by inducing infrared activity (that is, the ability to emit and absorb infrared radiation) in an otherwise infrared-inactive phonon vibration (Fig. 1a,b), as well as modifying electron–light interactions by generating a tunable electronic bandgap^{17–23} (Fig. 1c,d). At the same time, electron–phonon interactions are also accompanying the electronic bandgap opening and phonon dipole changes^{10–12}. This tunable coupling among electrons, vibrations and light offers exciting opportunities in the exploration of new physical phenomena. One example is the control of quantum interference between vibration- and electron-mediated optical absorption (Fig. 1e), which provides an unusual tunable Fano system involving three different elementary excitations: photon, exciton and phonon.

A Fano resonance describes the quantum interference effects on the optical absorption through coupled discrete and continuum transitions, in which the excited eigenstates are mixtures of the discrete and continuum states^{1,2}. It gives rise to characteristic asymmetric lineshapes in absorption spectra¹. First introduced to describe atomic photo-ionization², the Fano lineshape has been observed ubiquitously in neutron scattering³, Raman scattering⁴, photo-absorption in quantum wells⁵ and electrical transport through nanostructures⁶. In particular, Fano lineshapes have been observed in the Raman spectra of a number of graphitic materials, such as graphite intercalation compounds²⁴, fullerene systems²⁵, doped carbon nanotube bundles²⁶ and metallic carbon nanotubes²⁷, and are believed to arise from interference between the G-mode phonons and either plasmons or a multi-phonon continuum.

However, a tunable Fano system characterized by controlled interference between distinct many-body excitations has been lacking up to now. Here, bilayer graphene provides a unique many-body system in which Fano interference between coupled phonon and electron–hole pair excitations can be realized and controlled through electrical gating. Unlike the relatively simple Fano resonances characterized by single-electron transitions in atoms and quantum dots, the bilayer graphene Fano resonance describes a collective phonon vibration coupled to a continuum of electron–hole excitations through electron–phonon interactions. Such coupling leads to new elementary excitations described by hybrid phonon–exciton states, in which the phonon ‘dressed’ with an exciton cloud has centre frequency, linewidth and infrared activity strongly renormalized by the many-body interactions. This hybrid phonon–exciton excitation and the associated tunable Fano resonance in bilayer graphene can be continuously tuned through electrical gating and described quantitatively using a tight-binding model. This microscopic understanding of the couplings between electron, phonon and light in bilayer graphene can lead to novel applications making use of the tunable bandgap of bilayer graphene.

In our studies, we used dual-gated bilayer graphene samples. Figure 1f shows an optical microscopy image of a typical device. A pristine Bernal stacked graphene bilayer has inversion symmetry (for example, in Fig. 1a, the mid-point between atom A in the upper layer and atom B in the lower layer is an inversion centre), but an electrical field normal to the graphene plane breaks this symmetry and profoundly changes the graphene electronic and vibrational properties. Electronically, bilayer graphene is intrinsically an undoped gapless semiconductor. A normal electrical field, however, induces a non-zero energy gap and charge carrier doping. These two key parameters, electronic bandgap (Δ) and carrier doping concentration (n), can be controlled independently in a dual-gate graphene device. This is achieved by controlling both the top and bottom displacement fields D_t and D_b with the corresponding gates (Fig. 1g); the discontinuity of the displacement field $\Delta D = D_b - D_t$ determines the carrier doping concentration, and the average displacement field $\bar{D} = (D_b + D_t)/2$ determines the tunable bandgap¹⁷ (see Supplementary Information). For phonon vibrations, we focus on the symmetric G-mode phonon^{12,28} (Fig. 1a). It carries zero dipole moment and is therefore infrared inactive in the pristine symmetric bilayer. A normal electric field, however, breaks the symmetry between the upper and lower layers, resulting in different charges on the carbon atoms at the

¹Department of Physics, University of California at Berkeley, Berkeley, California 94720, USA, ²School of Physical Science and Technology, Lanzhou University, Lanzhou 730000, China, ³Advanced Light Source Division, Lawrence Berkeley National Laboratory, Berkeley, California 94720, USA, ⁴Materials Science Division, Lawrence Berkeley National Laboratory, Berkeley, California 94720, USA, ⁵Earth Sciences Division, Lawrence Berkeley National Laboratory, Berkeley, California 94720, USA. [†]Present address: Department of Physics, Fudan University, Shanghai 200433, China (Y.Z.). [‡]These authors contributed equally to this work. *e-mail: fengwang76@berkeley.edu

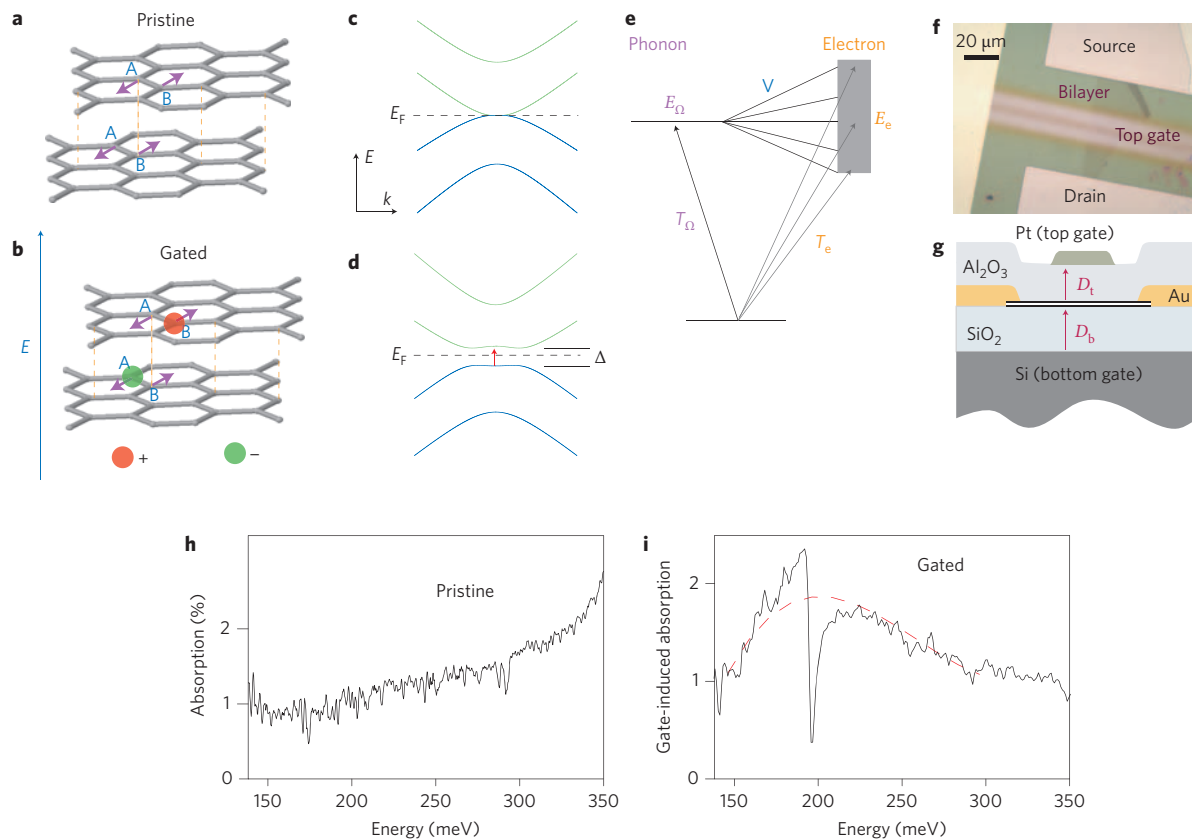


Figure 1 | Dual-gate bilayer graphene as a tunable Fano system. **a**, Symmetric optical phonon in a pristine A–B stacking graphene bilayer with zero dipole moment. **b**, Field-induced charge redistribution leads to infrared activity in the optical phonon. **c**, Pristine bilayer graphene with zero bandgap. **d**, An electrical field generates a finite bandgap in the bilayer graphene. **e**, Diagram of the Fano resonance describing the interfering infrared transitions to the coupled discrete phonon and continuum electronic states. **f**, Optical microscope image of a typical dual-gate graphene device. **g**, Illustration of the bilayer device, side view. **h**, Infrared absorption from a pristine bilayer. The absorption is relatively flat and no absorption resonance is present in this spectral range. **i**, Gate-induced infrared absorption spectrum of the bilayer graphene at zero doping and 190-meV bandgap energy. The broad absorption peak (fitted by a polynomial function in the red dashed curve) arises from bandgap electronic transitions. The sharp spectral feature at 195 meV is due to the optical phonon. The phonon resonance appears as a dip rather than an absorption peak because of Fano interference.

A site of the bottom layer and the B site of the top layer (Fig. 1b). These atoms now appear like oppositely charged ions in a polar crystal, and their vibrations become infrared active. A related phenomenon in which the Raman inactive antisymmetric G-mode phonon becomes Raman active due to the breaking of an inversion symmetry has been observed recently in single-gated bilayer graphene²⁹.

The field-induced electronic bandgap and phonon infrared activity lead to dramatic changes in graphene bilayer infrared absorption spectra. Figure 1h displays the absorption spectrum of an ungated bilayer sample, whereas Fig. 1i shows the gate-induced absorption spectrum with carrier doping $n \approx 0$ and bandgap $\Delta \approx 190$ meV. Although the ungated bilayer absorption spectrum is largely featureless, the spectrum with $\Delta \approx 190$ meV shows two prominent new features: a broad absorption peak corresponding to electronic bandgap transitions and a sharp spectral feature at 195 meV coincident with the G-phonon energy. Instead of seeing an absorption peak as might be expected for an infrared active phonon, we observe a strong absorption dip at the phonon frequency. This ‘anti-resonance’ signifies that the phonon and electronic excitations are not independent in bilayer graphene. Instead, they form a new elementary excitation of a hybrid phonon–exciton nature. Such new elementary excitations strongly modify light absorption around the phonon resonance. This can be described as a many-body realization of the Fano interference, in which the discrete state is the phonon vibration and the continuum states are the electron–hole pair excitations.

Phenomenologically, the absorption $A(E)$ at a given energy E under Fano resonance condition has a lineshape described by

$$A(E) = A_e \cdot \frac{[q \cdot \gamma + (E - E_\Omega)]^2}{(E - E_\Omega)^2 + \gamma^2}$$

(ref. 1), where A_e is the bare electronic state absorption, and E_Ω and γ are the centre energy and width of the phonon resonance, respectively. In the numerator, γ and $(E - E_\Omega)$ describe the phonon and electronic weights in the hybrid wavefunction at different energies, and the dimensionless parameter q characterizes the relative dipole strength of the renormalized phonon and electron transitions. Depending on the value of q , the absorption lineshape can include a resonance ($|q| \gg 1$, phonon dominates), dispersion ($|q| \approx 1$, comparable phonon and electron contribution) or anti-resonance ($|q| \ll 1$, electrons dominate). In bilayer graphene we can achieve these different lineshapes by controlling the electron and phonon transition dipoles with different gate electrical fields.

Figure 2a presents the Fano resonance absorption at different bandgap energies (Δ) and zero electron doping (black lines). To focus on the sharp Fano features, we have subtracted the broad electronic absorption background, which was approximated by a third-order polynomial fitting of the absorption in the frequency range 150–260 meV excluding the phonon region of 185–215 meV

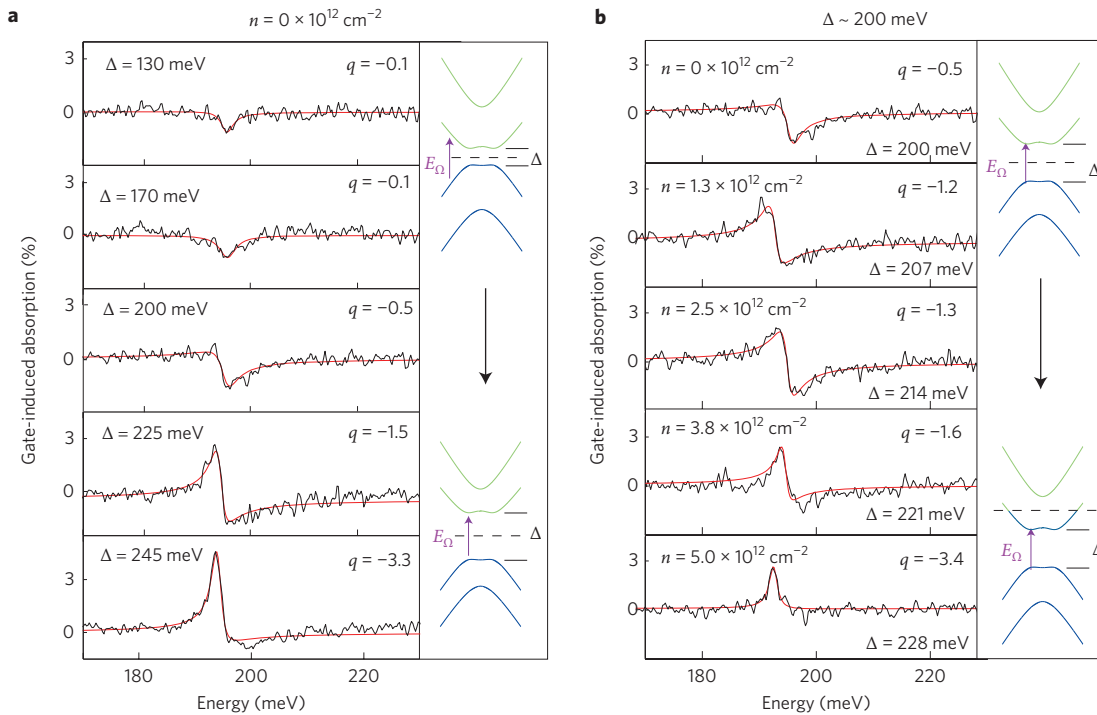


Figure 2 | Infrared absorption spectra of the gate-tunable Fano resonance. **a**, Controlling Fano resonance by varying the bandgap energy Δ (right panel). From top to bottom, Fano resonance absorption spectra show the Fano q -factor increasing with increasing Δ . (Broad electronic absorption backgrounds are subtracted.) Black curves are experimental data and red curves are fits with Fano lineshape. The lineshape changes from an ‘anti-resonance’ to dispersive-like to a resonance, corresponding to a change of interference parameter $|q| \ll 1$ (dominated by electronic absorption with $\Delta < E_{\Omega}$) to $|q| \gg 1$ (dominated by phonon absorption with $\Delta > E_{\Omega}$). **b**, Controlling Fano resonance by increasing the electron concentration at $\Delta \approx 200$ meV (right panel). Different Fano lineshapes are observed with increasing electron doping, corresponding to an increase of $|q|$. This effect is mainly due to a reduction of electronic dipole strength, because the final states for electronic transitions E_{Ω} are Pauli blocked by doped electrons, as illustrated in the right panel.

(Fig. 1i, red dashed line). These absorption spectra are well described by the Fano lineshape

$$A(E) - A_e = A_e \cdot \left(\frac{[q \cdot \gamma + (E - E_{\Omega})]^2}{(E - E_{\Omega})^2 + \gamma^2} - 1 \right)$$

where A_e , q , E_{Ω} and γ are the fitting parameters (fits are shown in Fig. 2a as red traces). In the relatively narrow spectral range around the Fano resonance, A_e has been approximated as a constant. The Fano lineshape is seen to change dramatically when the energy gap Δ is increased, first as a weak absorption dip, then as a dispersive interference, and finally as an absorption peak. The critical parameter describing these lineshapes is q . In our system, this dimensionless quantity q is given by

$$q = \frac{1}{\pi D_{e-h}(E_{\Omega}) V_{e-ph}} \times \frac{\mu_{ph}}{\mu_{e-h}^0}$$

where $D_{e-h}(E_{\Omega})$ is the joint electron–hole pair density of states at the renormalized phonon energy, V_{e-ph} is the electron–phonon coupling strength, and μ_{ph} and μ_{e-h} are the optical matrix element (dipole moment) of the dressed phonon and that of an electron–hole pair, respectively¹. (See Supplementary Information for details on how q is obtained from the calculations.) In these spectra, q is negative and its magnitude increases by an order of magnitude as Δ increases. This increase of $|q|$ can be qualitatively understood by two effects. First, the phonon gains infrared activity from the field-induced symmetry breaking, and its dipole moment μ_{ph} increases monotonically with the field strength. Second, electronic transitions at $E = E_{\Omega}$ become weaker with increasing field

strength once the gap energy is larger than E_{Ω} , because the joint electron–hole pair density of states $D_{e-h}(E_{\Omega})$ becomes extremely small (although not zero as a result of finite electronic broadening).

Instead of varying the electronic bandgap, we can also modify the Fano resonance infrared absorption by changing the carrier concentration. This is achieved experimentally by fixing the bottom-gate voltage and sweeping the top-gate voltage. In such measurements, the bandgap also changes slightly, but the dominant effects are from carrier doping. Figure 2b shows Fano absorption spectra (with the broad electronic absorption background subtracted) at different carrier concentrations. It can be seen that electron doping can also lead to a continuous change from a dip to a peak in the absorption spectrum around the phonon energy. In this case, the increase in $|q|$ is mainly due to a reduction of electronic transition strength from Pauli blocking; with an increase in the electron density, the Fermi energy shifts up and the electronic transitions at E_{Ω} become forbidden when the final states for such transitions are already filled.

The detailed dependence of Fano resonance parameters on electrical gating reveals not only the changes of electron and phonon optical dipole strengths contained in A_e and q , but also the renormalization of the ‘dressed’ phonon vibration frequency E_{Ω} and broadening γ . Figure 3a–d (symbols) presents the experimental data for A_e , q , E_{Ω} and γ at different gap energies, with $n \approx 0$. All such behaviours of the tunable many-body Fano resonance can be described quantitatively in bilayer graphene by calculating the band structure using a tight-binding model and by introducing the creation operator of a hybrid phonon–exciton excitation $h_E^{\pm} = \sin \theta_E \cdot (A \cdot a^{\pm} + \sum_{E' \neq E} B \cdot d_{E'}^{\pm}) + \cos \theta_E \cdot d_E^{\pm}$. Here, d_E^{\pm} is the creation operator of a specific superposition of electron–hole pair states at energy E , a^{\pm} creates a bare phonon, and A , B and θ_E are

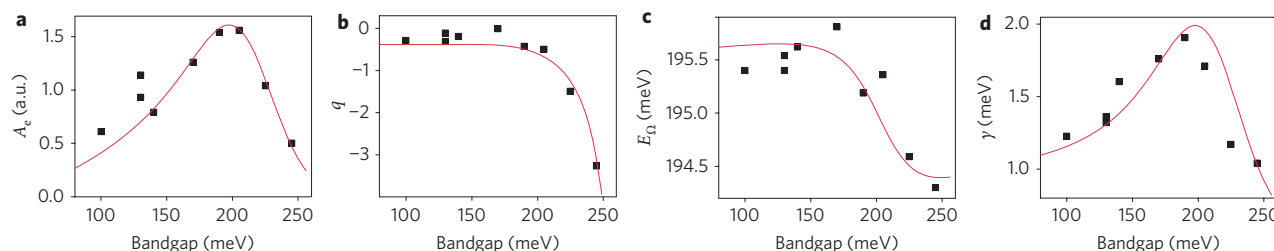


Figure 3 | Fano parameters as a function of tunable bandgap in undoped bilayer graphene. Symbols are experimental values and red lines are theoretical predictions. **a**, A_e describes the electronic infrared absorption at phonon frequency E_Ω . It reaches a maximum as the bandgap Δ approaches E_Ω . **b**, Fano parameter q describing the relative dipole strengths of phonon and electronic infrared transitions. The optical phonon acquires its dipole through field-induced symmetry breaking and increases monotonically, whereas the electronic dipole moment reaches its maximum at $\Delta = E_\Omega$. Consequently, $|q|$ increases dramatically at $\Delta > E_\Omega$. q is negative because coupling to electronic transitions with energy larger than Δ is stronger. **c**, Phonon vibration frequency decreases at larger gap energies. This phonon softening also arises from stronger coupling to electronic transitions with energy larger than Δ . **d**, Phonon linewidth is broadened by electron–phonon coupling. The linewidth reaches a maximum at $\Delta = E_\Omega$ when the electron–phonon interactions are the strongest.

energy-dependent parameters (see Supplementary Information for details)¹. The first term in the expression describes the renormalized phonon vibration, which is a bare phonon dressed by off-resonance electron–hole pair excitations. It is through this coupling that the phonon gains infrared activity.

Figure 3 presents a comparison of experimental values (symbols) and theoretical results (lines). We have used an energy broadening of 40 meV for the electronic transitions to account for the finite excited state lifetime and inhomogeneity in environmental carrier doping from charged impurities. A bare phonon energy of 197.1 meV and width of 0.6 meV in the absence of electron–phonon interactions were used as fitting parameters in Fig. 3c and d, respectively. Our fitting is consistent with tight-binding parameters of an intralayer hopping energy of 3 eV, an interlayer hopping energy of 0.4 eV, and vibration-induced hopping energy change of 6 eV \AA^{-1} (refs 10,30). Note some interesting relations between the Fano parameters. The phonon frequency is redshifted, and q assumes a negative value in this coupled electron–phonon system. These features are both a result of the fact that the phonon coupling to higher energy continuum states is greater than the coupling to lower energy states. Phonon width (γ) and electronic absorption (A_e) also show a common maximum when the bandgap energy is tuned close to the phonon energy (at 195 meV), both due to a dramatic increase in the electronic density of states. The additional broadening of the phonon width due to electron–phonon coupling reaches 1.4 meV, which is significantly larger than its intrinsic width of 0.6 meV. Similar broadening of phonon linewidth due to electron–phonon interactions has also been observed previously in Raman spectra of single-gated bilayer graphene^{12,29,31}. This corresponds to a maximum phonon decay rate of 4.2 ps^{-1} from electron–hole pair generation and 1.8 ps^{-1} from anharmonic phonon coupling.

In conclusion, gated bilayer graphene shows rich Fano resonance behaviour. It features coupled resonant light, exciton and phonon excitations enabled by electric field tuning. The unique tunable bandgap and strong electron–phonon interactions in bilayer graphene offer the possibility of a phonon laser, which can be easily appreciated from the analogy to its photon counterpart as in semiconductor lasers. In a semiconductor laser, photons with energy matching the electronic bandgap are amplified by stimulated emission from population-inverted bandgap electrons. Similarly, when the phonon energy matches the electronic bandgap as realized here, stimulated amplification and lasing of phonons can be achieved through bandgap electron population inversion. This simple scheme makes use of the unusual tunable electronic bandgap and is distinctly different from previous phonon laser proposals^{32–34}. The maximum ‘phonon gain’ in our system is set by the stimulated phonon emission rate (from fully population

inverted electrons), which equals the phonon absorption rate by unexcited electrons and is $\sim 4.2 \text{ ps}^{-1}$. In comparison, the ‘phonon loss’ is determined by the anharmonic phonon decay rate at $\sim 1.8 \text{ ps}^{-1}$. Therefore a phonon laser with stimulated phonon emission gain overcoming the loss can be achieved in bilayer graphene if sufficient population inversion is created by either optical pumping or electron injection.

Note added in proof: After submission of our paper, a related study of Fano resonance in doped bilayer graphene was reported³⁵.

Methods

The fabrication procedure for creating the dual-gate devices is described in ref. 17. Briefly, bilayer graphene was connected to 20-nm-thick gold source and drain electrodes. The doped silicon substrate under a 285-nm-thick SiO_2 layer served as the bottom gate, and a semi-transparent strip of platinum film on top of an 80-nm-thick Al_2O_3 film formed the top gate. The gold and platinum electrodes were deposited through stencil masks in vacuum. A cross-sectional view of the bilayer device is presented in Fig. 1g. Infrared absorption of the Fano resonance was measured using the synchrotron-based infrared source from the Lawrence Berkeley National Lab Advanced Light Source and a micro-Fourier transform infrared spectrometer. All experiments were carried out at room temperature.

Received 21 July 2009; accepted 1 October 2009;
published online 15 November 2009

References

- Fano, U. Effects of configuration interaction on intensities and phase shifts. *Phys. Rev.* **124**, 1866–1878 (1961).
- Fano, U. & Rau, A. R. P. *Atomic Collisions and Spectra* (Academic Press, 1986).
- Adair, R. K., Bockelman, C. K. & Peterson, R. E. Experimental corroboration of the theory of neutron resonance scattering. *Phys. Rev.* **76**, 308 (1949).
- Cerdeira, F., Fjeldly, T. A. & Cardona, M. Effect of free carriers on zone-center vibrational modes in heavily doped p-type Si. 2. Optical modes. *Phys. Rev. B* **8**, 4734–4745 (1973).
- Faist, J., Capasso, F., Sirtori, C., West, K. W. & Pfeiffer, L. N. Controlling the sign of quantum interference by tunnelling from quantum wells. *Nature* **390**, 589–591 (1997).
- Gores, J. *et al.* Fano resonances in electronic transport through a single-electron transistor. *Phys. Rev. B* **62**, 2188–2194 (2000).
- Zhang, Y. B., Tan, Y. W., Stormer, H. L. & Kim, P. Experimental observation of the quantum Hall effect and Berry’s phase in graphene. *Nature* **438**, 201–204 (2005).
- Novoselov, K. S. *et al.* Two-dimensional gas of massless Dirac fermions in graphene. *Nature* **438**, 197–200 (2005).
- Ferrari, A. C. *et al.* Raman spectrum of graphene and graphene layers. *Phys. Rev. Lett.* **97**, 187401 (2006).
- Yan, J., Zhang, Y. B., Kim, P. & Pinczuk, A. Electric field effect tuning of electron–phonon coupling in graphene. *Phys. Rev. Lett.* **98**, 166802 (2007).
- Pisana, S. *et al.* Breakdown of the adiabatic Born–Oppenheimer approximation in graphene. *Nature Mater.* **6**, 198–201 (2007).
- Yan, J., Henriksen, E. A., Kim, P. & Pinczuk, A. Observation of anomalous phonon softening in bilayer graphene. *Phys. Rev. Lett.* **101**, 136804 (2008).
- Wang, F. *et al.* Gate-variable optical transitions in graphene. *Science* **320**, 206–209 (2008).

14. Mak, K. F. *et al.* Measurement of the optical conductivity of graphene. *Phys. Rev. Lett.* **101**, 196405 (2008).
15. Li, Z. Q. *et al.* Dirac charge dynamics in graphene by infrared spectroscopy. *Nature Phys.* **4**, 532–535 (2008).
16. Kuzmenko, A. B., van Heumen, E., Carbone, F. & van der Marel, D. Universal optical conductance of graphite. *Phys. Rev. Lett.* **100**, 117401 (2008).
17. Zhang, Y. *et al.* Direct observation of a widely tunable bandgap in bilayer graphene. *Nature* **459**, 820–823 (2009).
18. McCann, E. Asymmetry gap in the electronic band structure of bilayer graphene. *Phys. Rev. B* **74**, 161403 (2006).
19. Ohta, T., Bostwick, A., Seyller, T., Horn, K. & Rotenberg, E. Controlling the electronic structure of bilayer graphene. *Science* **313**, 951–954 (2006).
20. Castro, E. V. *et al.* Biased bilayer graphene: semiconductor with a gap tunable by the electric field effect. *Phys. Rev. Lett.* **99**, 216802 (2007).
21. Guinea, F., Neto, A. H. C. & Peres, N. M. R. Electronic states and Landau levels in graphene stacks. *Phys. Rev. B* **73**, 245426 (2006).
22. Lu, C. L., Chang, C. P., Huang, Y. C., Chen, R. B. & Lin, M. L. Influence of an electric field on the optical properties of few-layer graphene with AB stacking. *Phys. Rev. B* **73**, 144427 (2006).
23. Oostinga, J. B., Heersche, H. B., Liu, X. L., Morpurgo, A. F. & Vandersypen, L. M. K. Gate-induced insulating state in bilayer graphene devices. *Nature Mater.* **7**, 151–157 (2008).
24. Eklund, P. C. & Subbaswamy, K. R. Analysis of Breit–Wigner line-shapes in the Raman-spectra of graphite-intercalation compounds. *Phys. Rev. B* **20**, 5157–5161 (1979).
25. Wang, Z. H., Dresselhaus, M. S., Dresselhaus, G. & Eklund, P. C. Raman studies of electron–phonon interaction in Kxc70. *Phys. Rev. B* **48**, 16881–16884 (1993).
26. Rao, A. M., Eklund, P. C., Bandow, S., Thess, A. & Smalley, R. E. Evidence for charge transfer in doped carbon nanotube bundles from Raman scattering. *Nature* **388**, 257–259 (1997).
27. Brown, S. D. M. *et al.* Origin of the Breit–Wigner–Fano lineshape of the tangential G-band feature of metallic carbon nanotubes. *Phys. Rev. B* **63**, 155414 (2001).
28. Ando, T. & Koshino, M. Field effects on optical phonons in bilayer graphene. *J. Phys. Soc. Jpn* **78**, 034709 (2009).
29. Malard, L. M., Elias, D. C., Alves, E. S. & Pimenta, M. A. Observation of distinct electron–phonon couplings in gated bilayer graphene. *Phys. Rev. Lett.* **101**, 257401 (2008).
30. Lazzeri, M., Piscanec, S., Mauri, F., Ferrari, A. C. & Robertson, J. Phonon linewidths and electron–phonon coupling in graphite and nanotubes. *Phys. Rev. B* **73**, 155426 (2006).
31. Das, A. *et al.* Phonon renormalization in doped bilayer graphene. *Phys. Rev. B* **79**, 155417 (2009).
32. Wallentowitz, S., Vogel, W., Siemers, I. & Toschek, P. E. Vibrational amplification by stimulated emission of radiation. *Phys. Rev. A* **54**, 943–946 (1996).
33. Liu, H. C. *et al.* Coupled electron–phonon modes in optically pumped resonant intersubband lasers. *Phys. Rev. Lett.* **90**, 077402 (2003).
34. Bargatin, I. & Roukes, M. L. Nanomechanical analog of a laser: amplification of mechanical oscillations by stimulated Zeeman transitions. *Phys. Rev. Lett.* **91**, 138302 (2003).
35. Kuzmenko, A. B. *et al.* Gate tunable infrared phonon anomalies in bilayer graphene. *Phys. Rev. Lett.* **103**, 116804 (2009).

Acknowledgements

This work was supported by the University of California at Berkeley and the Office of Basic Energy Sciences, US Department of Energy under contract no. DE-AC03-76SF0098 (Materials Science Division) and contract no. DE-AC02-05CH11231 (Advanced Light Source). Y.Z. and F.W. acknowledge support from a Miller Fellowship and a Sloan Fellowship, respectively. T.T.T. is partially supported by the National Science Council, Taiwan.

Author contributions

F.W. designed the experiment. T.T.T., Y.Z., B.G. and C.G. fabricated the sample. T.T.T., Y.Z., Z.H., M.C.M. and F.W. performed infrared spectroscopy measurements. C.H.P., S.G.L. and F.W. carried out the calculations. T.T.T., Y.Z., C.H.P., A.Z., M.F.C., S.G.L., Y.R.S. and F.W. co-wrote the paper.

Additional information

The authors declare no competing financial interests. Supplementary information accompanies this paper at www.nature.com/naturenanotechnology. Reprints and permission information is available online at <http://npg.nature.com/reprintsandpermissions/>. Correspondence and requests for materials should be addressed to F.W.